Research Note

On the error behaviour of force and moment sources in simplicial spectral finite elements

Mulder, W. A.

DOI
10.1111/1365-2478.13013

Publication date
2020

Document Version
Accepted author manuscript

Published in
Geophysical Prospecting

Citation (APA)
Mulder, W. A. (2020). Research Note: On the error behaviour of force and moment sources in simplicial spectral finite elements. *Geophysical Prospecting*, *68*(8), 2598-2603. https://doi.org/10.1111/1365-2478.13013

Geophysical Prospecting, 2020, **XX,** 000–000

Research Note: On the error behaviour of force and moment sources in simplicial spectral finite elements

W.A. Mulder[1,2]

[1]*Shell Global Solutions International B.V.,*
P.O. Box 38000, 1030 BN Amsterdam, The Netherlands
[2]*Department of Geoscience & Engineering, Faculty of Civil Engineering and Geosciences,*
Delft University of Technology, P.O. Box 5048, 2600 GA Delft, The Netherlands

Received April 2020, revision accepted July 2020

SUMMARY

The representation of a force or moment point source in a spectral finite-element code for modelling elastic wave propagation becomes fundamentally different in degenerate cases where the source is located on the boundary of an element. This difference is related to the fact that the finite-element basis functions are continuous across element boundaries, but their derivatives are not. A method is presented that effectively deals with this problem. Tests on 1-D elements show that the numerical errors for a force source follow the expected convergence rate in terms of the element size, apart from isolated cases where superconvergence occurs. For a moment source, the method also converges but one order of accuracy is lost, probably because of the reduced regularity of the problem. Numerical tests in 3D on continuous mass-lumped tetrahedral elements show a similar error behaviour as in the 1-D case, although in 3D, the loss of accuracy for the moment source is not a severe as a full order.

Key words: Computing aspects, Elastics, Modelling, Mathematical formulation, Seismics

Introduction

In exploration geophysics, the method of choice for elastic wave propagation modelling and inversion is the finite-difference method, whereas in seismology, the spectral element method on hexahedra (Komatitsch and Vilotte 1998) has found widespread use. On simplicial elements such as triangles and tetrahedra, the construction of spectral elements is not as straightforward as on quadrilaterals and hexahedra, where Cartesian products enable the generalization of the 1-D polynomial elements with Legendre-Gauss-Lobatto nodes and their corresponding quadrature weights to multiple dimensions. Up till now, triangular spectral elements of degree 2 and 3 (Tordjman 1995; Cohen *et al.* 1995, 2001), 4 (Mulder 1996), 5 (Chin-Joe-Kong *et al.* 1999), infinitely many of degree 6 (Mulder 2013), and 7 to 9 (Cui *et al.* 2017; Liu *et al.* 2017) have been found. Spectral elements for tetrahedra have been available since 1996 (Mulder 1996; Chin-Joe-Kong *et al.* 1999) but were rarely used because the requirement to maintain spatial accuracy after mass lumping comes at a high computational expense (Lesage *et al.* 2010; Mulder and Shamasundar 2016). This changed fairly recently, when a sharper accuracy criterion led to a significant cost reduction (Geevers *et al.* 2018, 2019), making them more appealing for large-scale applications.

The numerical representation of the source term in a finite-element method is straightforward if a point force source is considered. Integration of a spatial delta function against the finite-element basis functions provides the result in the form of weights equal to the basis functions evaluated at the source position (Komatitsch and Vilotte 1998). Degenerate cases where the source is located on a face, edge, or vertex of an element, do not pose a problem because the basis functions are continuous across elements. Therefore, evaluation with reference to one element or to another, either one having the source on its boundary, will provide the same weights as long as only a *single* element is considered per source. For a moment source, this is no longer true.

The problem arises when a moment source is represented by means of derivatives of delta functions. Integration against the finite-element basis functions then provides their derivatives at the source position. These are *not* continuous across element boundaries. If the source is, for instance, located on a face shared by two elements, a completely different result is obtained if the evaluation is carried out with reference to the element on one side of that face or on its other side.

A solution is presented below, together with a set of tests in one and three space dimensions to study its impact on the numerical accuracy. In 1D, the spectral elements consist of polynomials up to a certain degree, defined on Legendre-Gauss-Lobatto nodes to allow for mass lumping and explicit time stepping. The generalization to quadrilaterals in 2D and hexahedra in 3D involves Cartesian products of basis functions and is straightforward. Here, their formulation on tetrahedra is examined with polynomials of degree 1 to 4, but augmented with higher-degree polynomials in the interior of the faces and of the tetrahedral elements, which is required to maintain accuracy after mass lumping.

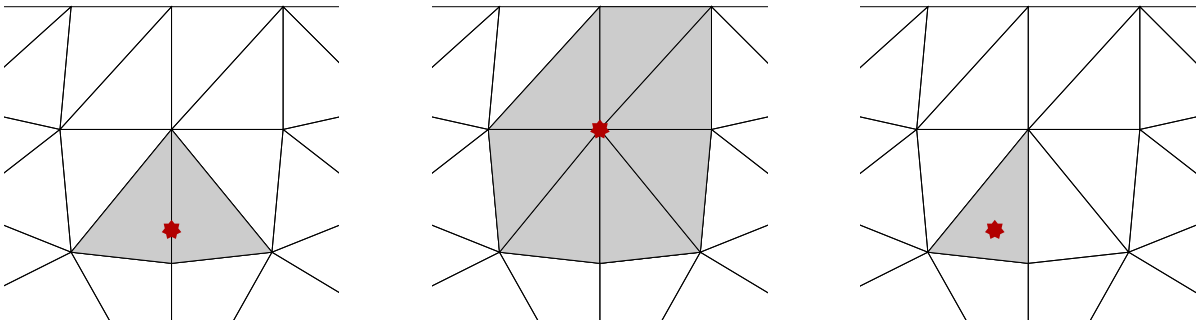

(a) (b) (c)

Figure 1. Three cases for the position of a moment source on a 2-D triangular mesh. If the source, marked by a star, lies inside a triangle (a), only one element is involved. If on an edge (b), two elements have to be considered. If on a vertex, all neighbouring elements have to be taken into account.

Method

Consider a computational domain Ω partitioned into simplicial elements $\mathcal{T}_j$ ($j = 1, \ldots, n_{\text{elem}}$). On each element, the basis functions $\phi_{j,k}$ are the Lagrange interpolating polynomials over the nodes $k = 1, \ldots, n_p$ of that element, obeying $\phi_{j,i}(x_k) = \delta_{i,k}$. In the finite-element discretization of the second-order form of the elastic wave equation, the basis functions provide the mass matrix $\boldsymbol{\mathcal{M}}$ and stiffness matrix $\boldsymbol{\mathcal{K}}$, as well as a discrete representation of the source term, $\mathbf{f}$ (Komatitsch and Vilotte 1998; Fichtner 2011; Mulder and Shamasundar 2016, e.g.).

A point force source is of the form $\mathbf{f} = w(t)\mathbf{s}\,\delta(\mathbf{x} - \mathbf{x}_s)$, where $w(t)$ denotes the wavelet, $\mathbf{s}$ its directional amplitudes, and $\mathbf{x}_s$ the source position. If the source is contained well inside an element j_s, as sketched in Figure 1(a) for the two-dimensional case, the contribution to $f_{g(j_s,k),\ell}$ is $\int_{\mathcal{T}_{j_s}} f_\ell \phi_{j_s,k}\,\mathrm{d}\mathbf{x} = w(t)s_\ell\phi_{j_s,k}(\mathbf{x}_s)$. Here, $g(j,k)$ defines the local-to-global map from node k in element j to the global set of degrees of freedom and $\ell = 1, 2, 3$ denotes the component.

If the source happens to lie on an edge, as sketched in Figure 1(b), there are two neighbouring elements j_1 and j_2 that contribute with weights $\phi_{j_1,k}(\mathbf{x}_s) = \phi_{j_2,k}(\mathbf{x}_s)$. These weights are equal, because the basis functions are assumed to be continuous from element to element. As a result, the source is counted twice. This can be repaired either by allowing only one element to contribute, which is the simplest approach, or by computing the sum of the contributing $\phi_{j,k}(\mathbf{x}_s)$ and dividing by it. That is, determine $a_i = \sum_{g(j,k)=i} \phi_{j,k}(\mathbf{x}_s)$, and divide $f_{i,\ell}$ by a_i if non-zero. In the case sketched in Figure 1(c), the source is located on a vertex and again only one element can be used to compute the discrete source term, or the normalization has to be carried out using all elements connected to that vertex, which will provide the same result but is clearly less efficient.

A point moment source has components of the form $w(t)M_{\ell,m}\partial_{x_m}\delta(\mathbf{x} - \mathbf{x}_s)$. If the source is well inside an element $\mathcal{T}_{j_s}$, the contribution to $f_{g(j_s,k),\ell}$ is

$$\int_{\mathcal{T}_{j_s}} \phi_{j_s,k} w(t) M_{\ell,m}\partial_{x_m}\delta(\mathbf{x} - \mathbf{x}_s)\,\mathrm{d}\mathbf{x} = -w(t)M_{\ell,m}\partial_{x_m}\phi_{j_s,k}(\mathbf{x}_s). \tag{1}$$

This involves derivatives of the basis functions evaluated at the source position. Because these are not continuous across element boundaries, the simple approach of evaluating the source term for just a single element will fail in the cases of Figure 1(b,c). Then, the alternative method of adding contributions for all neighbouring elements and normalizing by a_i, if non-zero, is needed. Note that the latter involves the values of the basis functions, not their derivatives.

The net result for component ℓ of the finite-element source term at the node with global index i, is

$$f_{i,\ell} = \frac{1}{a_i} \sum_{g(j_s,k)=i} f_{g(j_s,k),\ell} \quad \text{if } a_i \neq 0, \tag{2a}$$

$$f_{g(j_s,k),\ell} = w(t)s_\ell\phi_{j_s,k}(\mathbf{x}_s) - w(t)\sum_{m=1}^{3} M_{\ell,m}\partial_{x_m}\phi_{j_s,k}(\mathbf{x}_s), \tag{2b}$$

$$a_i = \sum_{g(j_s,k)=i} \phi_{j_s,k}(\mathbf{x}_s). \tag{2c}$$

If $a_i = 0$, then $f_{i,\ell} = 0$. Here, force and moment sources have been combined into one expression, but usually only one of them is present. One or more elements $\mathcal{T}_{j_s}$ contain the source position $\mathbf{x}_s$, the wavelet is $w(t)$, the force source has elements s_ℓ and the symmetric moment source tensor $M_{\ell,m}$ for $\ell = 1, 2, 3$ and $m = 1, 2, 3$. The nodes are enumerated by $k = 1, \ldots, n_p$ inside one element $\mathcal{T}_j$ with associated Lagrange basis functions $\phi_{j,k}$, and $g(j,k)$ defines the local-to-global map from node k in element j to the global set of nodes or scalar degrees of freedom.

Since the examples involve higher-order time stepping (von Kowalevsky 1875; Lax and Wendroff 1960; Dablain 1986; Shubin and Bell 1987; Mulder *et al.* 2014), the related equations are recapitulated for completeness. For order M_t, we have

$$\mathbf{u}^{n+1} - 2\mathbf{u}^n + \mathbf{u}^{n-1} = 2\sum_{m=1}^{M_t/2} \frac{(\Delta t)^{2m}}{(2m)!}\frac{\partial^{2m}\mathbf{u}^n}{\partial t^{2m}}, \tag{3a}$$

$$\frac{\partial^{2m+2}\mathbf{u}^n}{\partial t^{2m+2}} = \boldsymbol{\mathcal{M}}^{-1}\left(\frac{\partial^{2m}\mathbf{f}^n}{\partial t^{2m}} - \boldsymbol{\mathcal{K}}\frac{\partial^{2m}\mathbf{u}^n}{\partial t^{2m}}\right), \quad m \geq 0. \tag{3b}$$

The superscript n denotes the values at time $t^n = n\Delta t$. Higher-order time stepping can be avoided altogether, of course, with Stork's dispersion correction method (Stork 2013; Wang and Xu 2015; Anderson *et al.* 2015; Qin *et al.* 2017; Koene *et al.* 2017).

Numerical results in one dimension

The acoustic wave equation in terms of displacement rather than pressure reads

$$\rho\frac{\partial^2 u}{\partial t^2} = f + \frac{\partial}{\partial x}\left(\rho v^2\frac{\partial u}{\partial x}\right), \tag{4}$$

where the displacement $u(t,x)$ depends on time t and position x, $\rho(x)$ is the density and $v(x)$ the sound speed. As before, $f(t,x) = w(t)\delta(x - x_s)$ defines a point force source at x_s. For a moment source, the same expression with $f = -W(t)\partial_x\delta(x - x_s)$ can be used. The spectrum is similar in both cases if $W(t)$ is the time integral of the wavelet $w(t)$ for the force source. For a problem with constant coefficients and non-reflecting boundary conditions, the exact solution at sufficiently large time, after the wavelet has ended, is

$$u^f_{\text{exact}}(t,x) = \frac{1}{2\rho v}\Big[W\big(t-(x-x_s)/v\big) + W\big(t+(x-x_s)/v\big)\Big], \quad (5)$$

for a force source, whereas a moment source leads to

$$u^M_{\text{exact}}(t,x) = \frac{1}{2\rho v^2}\Big[W\big(t-(x-x_s)/v\big) - W\big(t+(x-x_s)/v\big)\Big]. \quad (6)$$

In one space dimension, the spectral elements are polynomials up to degree p defined on Legendre-Gauss-Lobatto nodes. The inclusion of the vertices makes them continuous and the choice of nodes provides sufficient accuracy after mass lumping. For the numerical tests, a domain with $x \in [0,2]$ km is partitioned into an even number of cells with constant width h. The shot is placed at $x_s = x_{j_s} + \xi_s h$ where $0 \le \xi_s < 1$ and $x_{j_s} = 1$ km is the position of a mesh vertex. The source wavelet is chosen either as a 10-Hz Ricker wavelet $w(t)$ for a force source or as its time integral $W(t)$ for a moment source. The sound speed is $v = 2$ km/s and the density is $\rho = 2$ g/cm^3. Time runs from 0 to 0.3 s.

The fourth-order central Lax-Wendroff time-stepping scheme ran at 80% of the maximum allowable time step. Together with a polynomial degree $p = 3$ for the spatial discretization, the solution error is expected to behave as $O(h^4)$ for an element size h, if the solution itself is sufficiently smooth and the mesh sufficiently fine.

Figure 2(a) displays the maximum and root-mean-square (RMS) error, relative to the maximum amplitude, as a function of mesh size h for a fixed relative source position $\xi_s = 0.2$. If a power-law fit is made, the error is roughly proportional to h^4 with the force source, both for the RMS and maximum error. With the moment source, one order is lost and we observe roughly $O(h^3)$ convergence.

Figure 2(b) displays the powers obtained by such power-law fits for various choices of the relative source position ξ_s, obtained with the RMS norm for a force or moment source. Figure 2(c) does the same for the maximum error. Results are fairly similar. For some choices of ξ_s, superconvergence is observed. The term 'superconvergence' is used here in the narrow sense of higher-order accuracy at isolated points (Strang and Fix 1973, p. 168).

For the force source, the peak in the measured power occurs near the Legendre-Gauss-Lobatto nodes, defined by the element's endpoints and the roots of the derivative of the Legendre polynomial, $\frac{\mathrm{d}}{\mathrm{d}x}P_3(x_j) = 0$, at $\zeta_j = \frac{1}{2}(1+x_j) = 0$, $\frac{1}{2}(1-\sqrt{1/5}) = 0.2764$, $\frac{1}{2}(1+\sqrt{1/5}) = 0.7236$, and 1. For the moment source, the peaks occur near the three roots of $P_3(x)$, at $\zeta_j = \frac{1}{2}(1+x_j) = \frac{1}{2}(1-\sqrt{3/5}) = 0.1127$, $\frac{1}{2}$, and $\frac{1}{2}(1+\sqrt{3/5}) = 0.8873$.

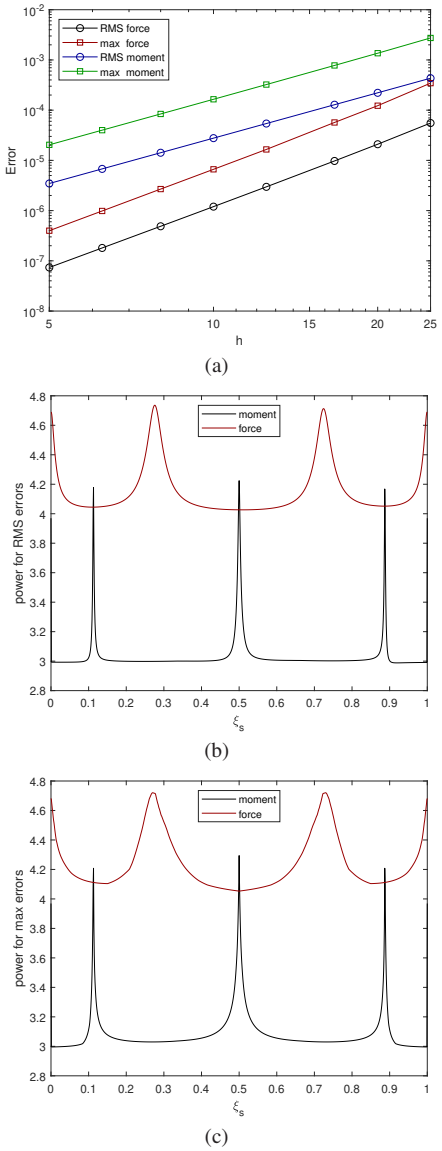

Figure 2. Powers for errors with 1-D elements of polynomial degree 3. (a) The RMS and maximum error as a function of element size h for a force or moment source at a fixed relative source position $\xi_s = 0.2$. Power-law fits provide the powers shown in (b) and (c) as a function of the relative source position ξ_s for the RMS and maximum errors, respectively.

Numerical results in three dimensions

The application to tetrahedra faces the same issues as the 1-D case. For the continuous mass-lumped finite elements, augmented with higher-degree polynomials to preserve accuracy after mass lumping, only the more efficient ones are considered, with 4 nodes for the standard linear elements, 15 for degree 2, 32 for 3 and 65 for degree 4 (Geevers *et al.* 2018, 2019).

The test problem resembled that of Geevers *et al.* (2019). The domain had $x \in [-2,2]$ km, $y \in [-1,1]$ km, and $z \in [0,2]$ km. The isotropic elastic parameters were constant, with P-wave velocity $v_p = 2.0$ km/s, S-wave velocity $v_s = 1.2$ km/s and density $\rho = 2$ g/cm^3. The source was positioned at $x_s = y_s = 0$ m and a depth $z_s = 1,000$ m. Receivers were placed between $x_r = -612.5$ to 612.5 m at a 25-m interval and at $y_r = 200$ and $z_r = 800$ m. The Ricker wavelet had a 5-Hz peak frequency for the vertical force source with $\mathbf{s} = (0\ 0\ 1)^{\mathsf{T}}$. For the moment source, the time integral of that Ricker wavelet was used and the moment tensor was

$$M = \begin{pmatrix} 0 & 2 & 1 \\ 2 & 0 & -1 \\ 1 & -1 & 0 \end{pmatrix}. \quad (7)$$

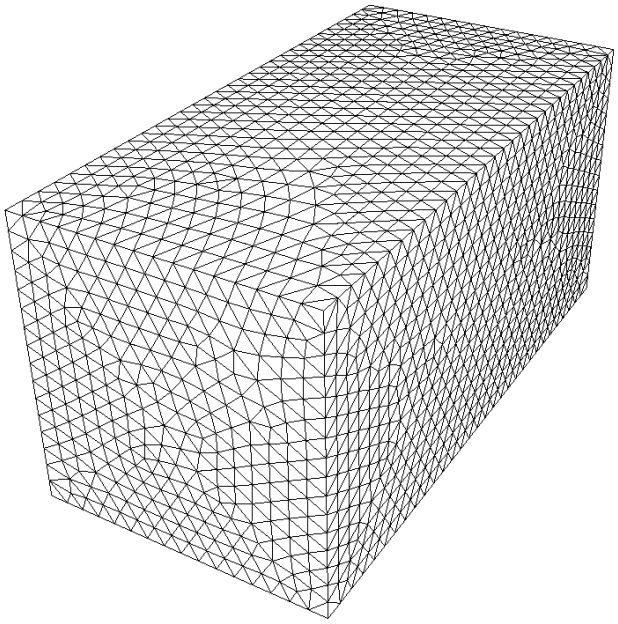

Figure 3. Example of a mesh.

Natural, reflecting boundaries were used on all sides. Time ran from −0.42 to 0.60 s, starting before the onset of the zero-phase wavelet and ending before reflections reached the receivers. A sequence of successively finer meshes was considered, with one shown in Figure 3.

Figure 4(a) displays the root-mean-square (RMS) errors for a force source, observed on several meshes with the four continuous mass-lumped finite-element schemes considered here, from degree $p = 1$ to 4. Power-law fits show that on average, the error behaves slightly better than h^{p+1}, where $N^{-1/3}$ was taken instead of the average element size h. Here, N is the total number of scalar degrees of freedom, which is one-third of the number of displacement unknowns. Figure 4(b) shows similar curves for the moment source. Power-law fits yield powers that are significantly smaller than $p + 1$ for elements with degrees $p = 1$ to 4, as in the 1-D case, although the loss of accuracy apparently is less than a full order for the higher degrees.

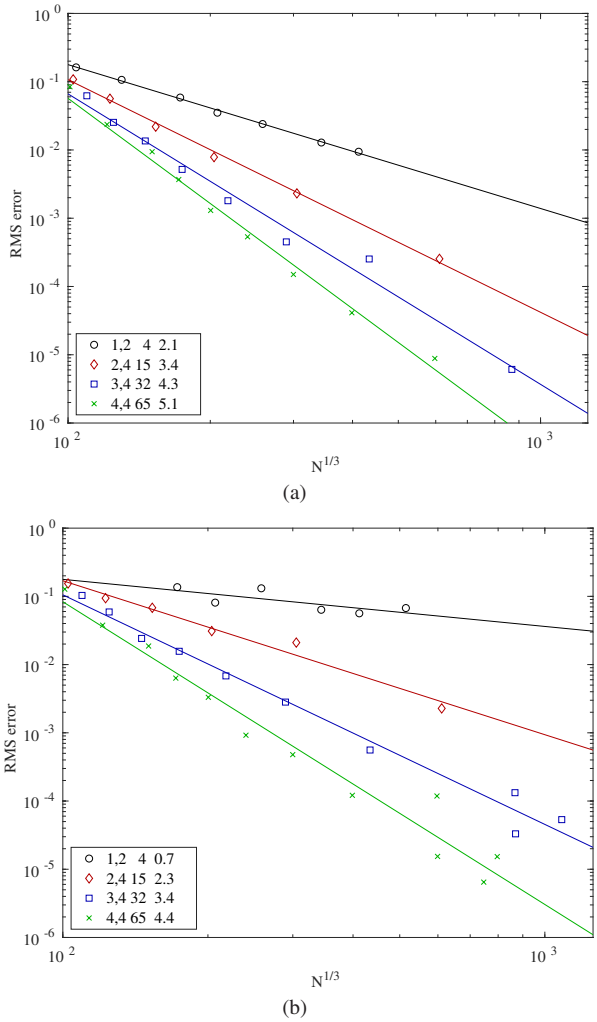

Figure 4. RMS errors for a 3-D homogeneous elastic problem with a force source (a) or moment source (b) as a function of the cube root of the number of scalar degrees of freedom N. The legend contains the polynomial degree of the finite-element discretization, the order of the time-stepping scheme, the number of nodes per element, and the power of the power-law fit to the error. The latter are included as drawn lines.

Conclusions

A solution was presented to the degeneracy of a moment source located on an element boundary. For a spectral element of a given degree, 1-D experiments show that a force source and a smooth wavelet produces errors of the order of the degree plus one, apart from isolated source positions at which superconvergence occurs. A moment source has one order less, most likely due to reduced regularity. The generalization to quadrilaterals in 2D and hexahedra in 3D is straightforward. In 3D on tetrahedra with continuous mass-lumped elements, a similar error behaviour was observed, establishing the validity of the approach.

REFERENCES

Anderson, J. E., Brytik, V., and Ayeni, G., 2015. Numerical temporal dispersion corrections for broadband temporal simulation, RTM and FWI, in *SEG Technical Program Expanded Abstracts*, pp. 1096–1100. doi:10.1190/segam2015-5817144.1

Chin-Joe-Kong, M. J. S., Mulder, W. A., and van Veldhuizen, M., 1999. Higher-order triangular and tetrahedral finite elements with mass lumping for solving the wave equation, *Journal of Engineering Mathematics*, **35**, 405–426. doi:10.1023/A:1004420829610

Cohen, G., Joly, P., and Tordjman, N., 1995. Higher order triangular finite elements with mass lumping for the wave equation, in *Proceedings of the Third International Conference on Mathematical and Numerical Aspects of Wave Propagation*, edited by G. Cohen, E. Bécache, P. Joly, and J. E. Roberts, pp. 270–279, SIAM, Philadelphia.

Cohen, G., Joly, P., Roberts, J. E., and Tordjman, N., 2001. Higher order triangular finite elements with mass lumping for the wave equation, *SIAM Journal on Numerical Analysis*, **38**(6), 2047–2078. doi:10.1137/S0036142997329554

Cui, T., Leng, W., Lin, D., Ma, S., and Zhang, L., 2017. High order mass-lumping finite elements on simplexes, *Numerical Mathematics: Theory, Methods and Applications*, **10**(2), 331–350. doi:10.4208/nmtma.2017.s07

Dablain, M. A., 1986. The application of high-order differencing to the scalar wave equation, *Geophysics*, **51**(1), 54–66. doi:10.1190/1.1442040

Fichtner, A., 2011. *Full Seismic Waveform Modelling and Inversion*, Springer-Verlag, Berlin, Heidelberg. doi:10.1007/978-3-642-15807-0

Geevers, S., Mulder, W. A., and van der Vegt, J. J. W., 2018. New higher-order mass-lumped tetrahedral elements for wave propagation modelling, *SIAM Journal on Scientific Computing*, **40**(5), A2830–A2857. doi:10.1137/18M1175549

Geevers, S., Mulder, W. A., and van der Vegt, J. J. W., 2019. Efficient quadrature rules for computing the stiffness matrices of mass-lumped tetrahedral elements for linear wave problems, *SIAM Journal on Scientific Computing*, **41**(2), A1041–A1065. doi:10.1137/18M1198557

Koene, E. F. M., Robertsson, J. O. A., Broggini, F., and Andersson, F., 2017. Eliminating time dispersion from seismic wave modeling, *Geophysical Journal International*, **213**(1), 169–180. doi:10.1093/gji/ggx563

Komatitsch, D. and Vilotte, J. P., 1998. The spectral-element method: an efficient tool to simulate the seismic response of 2-D and 3-D geological structures, *Bulletin of the Seismological Society of America*, **88**(2), 368–392.

Lax, P. and Wendroff, B., 1960. Systems of conservation laws, *Communications on Pure and Applied Mathematics*, **31**(2), 217–237. doi:10.1002/cpa.3160130205

Lesage, A. C., Aubry, R., Houzeaux, G., Polo, M. Araya, and Cela, J.M., 2010. 3D spectral element method combined with h-refinement, 72nd EAGE Conference & Exhibition, Barcelona, Spain, Extended Abstracts, C047. doi:10.3997/2214-4609.201400702

Liu, Y., Teng, J., Xu, T., and Badal, J., 2017. Higher-order triangular spectral element method with optimized cubature points for seismic wavefield modeling, *Journal of Computational Physics*, **336**, 458–480. doi:10.1016/j.jcp.2017.01.069

Mulder, W. A., 1996. A comparison between higher-order finite elements and finite differences for solving the wave equation, in *Proceedings of the Second ECCOMAS Conference on Numerical Methods in Engineering*, edited by J.-A. Désidéri, P. LeTallec, E. Oñate, J. Périaux, and E. Stein, pp. 344–350, John Wiley & Sons, Chichester.

Mulder, W. A., 2013. New triangular mass-lumped finite elements of degree six for wave propagation, *Progress In Electromagnetics Research*, **141**, 671–692. doi:10.2528/PIER13051308

Mulder, W. A. and Shamasundar, R., 2016. Performance of continuous mass-lumped tetrahedral elements for elastic wave propagation with and without global assembly, *Geophysical Journal International*, **207**(1), 414–421. doi:10.1093/gji/ggw273

Mulder, W. A., Zhebel, E., and Minisini, S., 2014. Time-stepping stability of continuous and discontinuous finite-element methods for 3-D wave propagation, *Geophysical Journal International*, **196**(2), 1123–1133. doi:10.1093/gji/ggt446

Qin, Y., Quiring, S., and Nauta, M., 2017. Temporal dispersion correction and prediction by using spectral mapping, in *79th EAGE Conference & Exhibition, Paris, France, Extended Abstracts, Th P1 10*. doi:10.3997/2214-4609.201700677

Shubin, G. R. and Bell, J. B., 1987. A modified equation approach to constructing fourth order methods for acoustic wave propagation, *SIAM Journal on Scientific and Statistical Computing*, **8**(2), 135–151. doi:10.1137/0908026

Stork, C., 2013. Eliminating nearly all dispersion error from FD modeling and RTM with minimal cost increase, in *75th EAGE Conference & Exhibition incorporating SPE EUROPEC, Extended Abstract*. doi:10.3997/2214-4609.20130478

Strang, G. and Fix, G., 1973. *An Analysis of the Finite Element Method*, Prentice-Hall, Inc., Englewood Cliffs, N.J.

Tordjman, N., 1995. *Élements finis d'order élevé avec condensation de masse pour l'equation des ondes*, Ph.D. thesis, L'Université Paris IX Dauphine.

von Kowalevsky, S., 1875. Zur Theorie der partiellen Differentialgleichung, *Journal für die reine und angewandte Mathematik*, **80**, 1–32. doi:10.1515/crll.1875.80.1

Wang, M. and Xu, S., 2015. Time dispersion transforms in finite difference of wave propagation, in *77th EAGE Conference & Exhibition, Extended Abstract*. doi:10.3997/2214-4609.201412619